Supplementary Material for

Boosting the electrochemical performance through proton transfer for the Zn-ion hybrid supercapacitor with both ionic liquid and organic electrolytes

Haitao Zhou†[a], Chao Liu†[a], Jianchun Wu†[a,c], Menghao Liu[a], Dong Zhang[a], Honglei Song[a], Xiaoyun Zhang[a], Hongquan Gao[a], Jianhong Yang*[a], and De Chen*[a, b]

[a] School of Materials Science and Engineering, Jiangsu University, 212013, Jiangsu Province, (P. R. China)

[b] Department of Chemical Engineering, Norwegian University of Science and Technology, N-7491, Trondheim, Norway

[c] Key Laboratory of Radiation Physics and Technology, Ministry of Education; Institute of Nuclear Science and Technology, Sichuan University, Chengdu 610064, China

† Dr. H. Zhou, Dr. J. Wu, and C. Liu contributed equally to this work.

---

* **Email**: [jhyang@ujs.edu.cn] (J. Yang); [de.chen@ntnu.no] (D.Chen);
Postal address: School of Materials Science and Engineering, Jiangsu University, No. 301, Xuefu Road, Zhenjiang, 212013, Jiangsu Province, (P. R. China)
Tel. +86 0511 88780856 **Fax:** +86 0511 88780856
† Dr. H. Zhou, Dr J. Wu and C. Liu contributed equally to this work.

Experimental and simulation

Materials synthesis

The Polyaniline (PANI) nanofiber was prepared from aniline monomer by a rapidly-mix method as our previous works. 1 mol L^{-1} HCl solution containing 30.0 g L^{-1} aniline (Sinopham, >99.5%) was mixed quickly with 1 mol L^{-1} HCl solution containing 18.4 g L^{-1} ammonia peroxydisulfate (Sinopham, >98%) oxidant with a volume ratio of 1:1. After stirring the mixture at 400 rad min^{-1} for 20 min, the PANI was separated by paper filtration, washed with water until a pH = 7 was reached and then dried in air overnight at 60 ˚C. Then, the PANI was carbonized in a quartz tube furnace by pyrolysis under 100 mL min^{-1} Ar flow. The heating rate of the furnace was set at 10 ˚C min^{-1}, and the maximum temperature was held at 650 ˚C for a 2 h dwelling. The carbonized PANI was grinded for 10 minute and then activated in quartz tube furnace under N_2 flow. The heating rate of furnace was set at 10 ˚C min^{-1}. When the temperature reached 800 ˚C, the steam was started to pump into the furnace with a high vapor partial pressure of 0.92 in the N_2/steam mixture (the mass ratio of H_2O/C is 4), and the heating rate was set at 5 ˚C min^{-1}. When the temperature reached 950 ˚C, the steam was switched to the CO_2 gas with a partial pressure of 0.6 in the N_2/CO_2 mixture. The maximum temperature was held at 950 ˚C for a 1 h dwelling to obtain the functionalized carbon nanosponges (FCNSs) sample.

The FCNSs samples were heat treated at different temperatures (200, 400, and 600 ˚C) for 4h. These samples are denoted as FCNSs200, FCNSs400, and FCNSs600 for short in the following. The carbon nanosponges (CNSs) sample was prepared by the KOH activation of carbonized PANI, as same as our previous work.

Material characterization

The microstructure and morphology of the FCNSs were characterized by the scanning electron microscopy (SEM, JEOL, JSM-7001F) and transmission electron microscopy (TEM, FEI TS20 microscope). The specific surface area and pore size distribution (PSD) were obtained from N_2 sorption (-196 ˚C) isothermals performed on a (MicrotracBEL, BELSORP-MAX) instrument with a relative pressure (P/P_0) of 0.00000001 to 1. The samples were degassed at 200 ˚C for 12 h under turbo molecular vacuum pumping prior to the gas adsorption measurements. The chemical compositions of the samples were detected by the element analysis (EA) using Elementar Vario MACRO cube. FTIR analyses of the functional groups were adopted by Nicolet iS50. X-ray photoelectron spectroscopy (XPS) analyses were performed on a Thermo ESCALAB 250XI spectrometer.

Electrochemical measurements

The positive electrode materials were prepared by milling the activated carbon powders (85 wt%) with 7 wt% Super-P carbon black and 8 wt% polytetrafluoroethylene binder (PTFE, Solvay). The electrode were fabricated by pressing the CNS-SP-PTFE mixture over an commercial carbon coated Al foil (FOILTEC, Honghua Electronics Co. Ltd, with a thickness of 12 μm and an areal density of 5.4 mg cm^{-2}) (**Fig. S1**) at 6 MPa for duration of 2 min. In fact, the carbon coated Al foils have been widely used as current collectors for high power Li-ion batteries and capacitors for their better contact with electrode materials than planar foils and the anticorrosion effect.[1] The electrodes were cut into circular electrodes with diameter of 12 mm. The mass loading of the cathode active material was approximately 2 mg cm^{-2}. The electrodes were dried in the vacuum oven at 120 ˚C

overnight before assembling in argon-filled glovebox. Both the FCNSs positive and Zn foil (Sinopham, 20 μm) negative electrodes were assessed with 2025 coin cells, by using a glass fiber film (Whatman, 934-AH^{TM}) as the separator. The electrolytes used were 0.2 M $Zn(CF_3SO_3)_2$ (Sinopham, >98%) in $EMIMCF_3SO_3$ (Sigma-Aldrich) and1 M $Zn(CF_3SO_3)_2$ in acetonitrile (AN) (Guotai Huarong, SCs grade). The prepared cells were stabilized overnight before the performance test. Cell assembly was carried out in an argon-filled glove box, in which water and oxygen concentrations were 0.1 ppm. For making a typical coffee-bag cell, the carbon electrode, an aromatic heterocyclic polymer-based separator (homemade) and Zn anode were punched into squares with 50 mm×30 mm, 55 mm×35 mm, and 50 mm×30 mm, respectively. Charge/discharge analysis was performed galvanostatically with an 8-channel battery analyzer (Neware, BTS-5V6A) at room temperature (T=25 ˚C). During the long-term cycling, a rest step time of 6 seconds was set between the charge and discharge.

The electrochemical impedance spectra (EIS) and cyclic voltammetry (CV) of the Zn-ion hybrid SCs were assessed using a 3-electrode cell (EL-CELL ECC-Ref Electrochemical Test Cell, Germany) with a tiny metallic Zn wire as the reference electrode. The electrochemical impedance spectra (EIS) were measured using a multi-channel potentiostat (PARSTAT MC, AMETEK) in the frequency range of 100 kHz to 10 mHz. The cyclic voltammetry (CV) data were collected with PARSTAT MC at a scanning rate of 10-1000 mV s^{-1}.

The gravimetric capacitance of the Zn-ion SCs was calculated from the galvanostatic discharge curve according to $C=(I\Delta t)\cdot(m\Delta V)^{-1}$, where I is the constant discharge current, m is the mass of cathode active materials on the electrodes, ΔV is the voltage change during the discharge process,

and Δt is the duration of the discharge process. The specific energy of the SCs (based on the mass of cathode active materials) were estimated as $E=C\cdot\Delta V^2/8$.

Computational details

The proton transition mechanisms on the FCNSs surface were demonstrated using density functional theory (DFT) calculations. All the calculations based on DFT were carried out using Vienna Ab initio Simulation Package (VASP). [2-4] The generalized gradient approximation (GGA) in the form of the Perdew, Burke, and Ernzerhof (PBE) functional was used to approximate the exchange and the correlation. The FCNSs surface (graphene oxide) models were built by cell parameters of $a=b=c$ =18 Å; $\alpha=\beta=\gamma=90^{\circ}$. The k-point meshes in the Brillouin zone (BZ) were sampled by 2×2×2. The convergence of plane-wave expansion was obtained with a cut-off energy of 400 eV. Gaussian smearing with a width of 0.05 eV was used for the occupation of the electronic levels. Electronic self-consistent energy had a convergence accuracy of 1×10^{-4} eV. All structures were optimized until the forces on all unconstrained atoms were less than 0.02 eV $Å^{-1}$.

The transition energy (E_{Tr}) of the proton transfer was calculated as

$$E_{Tr} = E_{tot} - \left(E_{GOH} + E_{OfT}\right) \quad (1)$$

where E_{tot} is the total energy of the system after the proton transfer; E_{GOH} is the energy of the graphene oxide of the FCNSs with a proton; and E_{OfT} is the energy of CF_3SO_3 group. A negative E_{Tr} value implies an energy favorable transition.

The charge density difference can be used to analyze the transfer of interatomic charge, and the charge accumulation regions and charge depletion regions are ascertained. The charge density difference was calculated by the equation as follows:[5]

$$\Delta\rho = \rho_{tot} - \rho_{GO} - \rho_{H} - \rho_{OfT} \quad (2)$$

Where ρ_{tot} is the total charge density of the graphene oxide-proton-CF_3SO_3 system; ρ_{GO}, ρ_{H}, and

ρ_{OfT} are the charge densities of isolated graphene oxide, proton and CF_3SO_3 group in the same combined structure.

Figs

Fig. S1

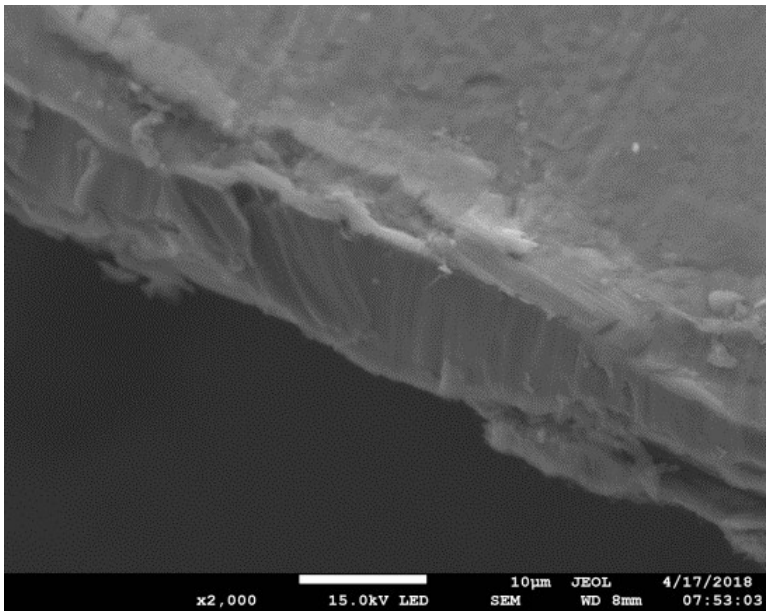

Fig. S1. SEM image of the carbon coated Al foil current collector acquired from a cross-section. This current collector has a thickness of 12 µm and 1µm high-purity graphite coating layers on both sides. The areal density is 5.4 mg cm^{-2}, which is as same as the commercial planar Al foil current collector.

Fig. S2

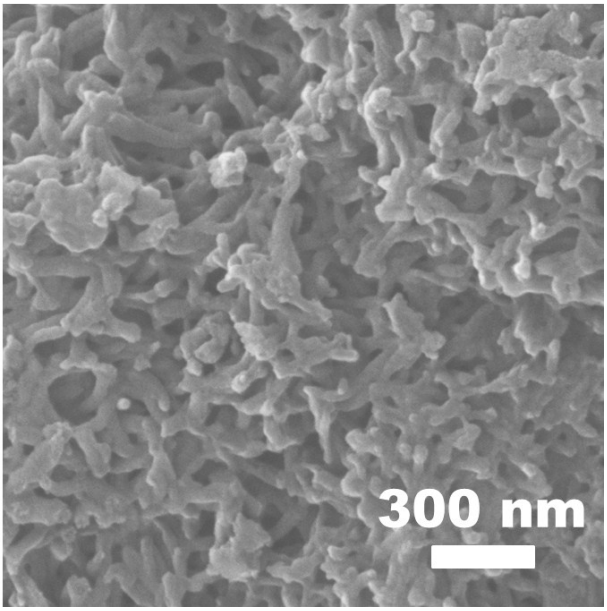

Fig. S2. SEM image of the CNSs materials with the bridged and linked fibers structure.

Fig. S3

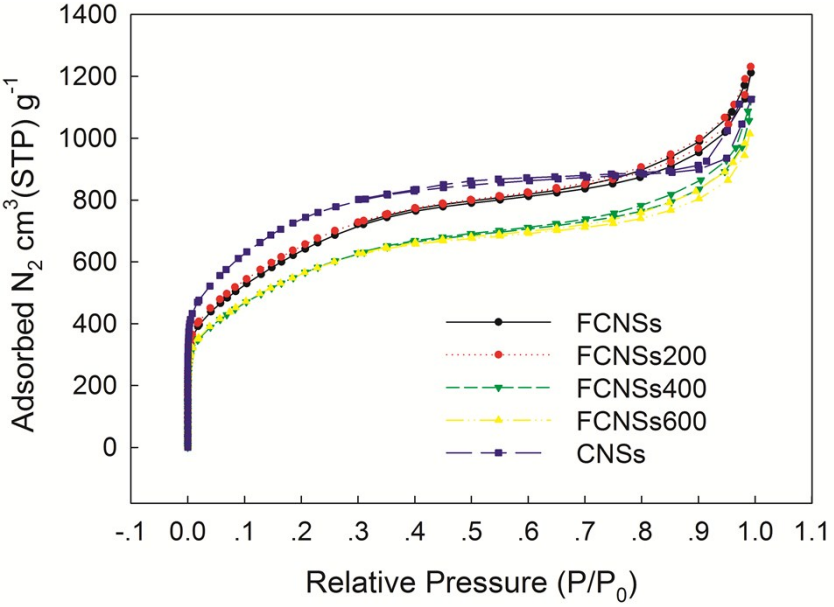

Fig. S3. N_2 isotherms of the FCNSs, FCNSs200, FCNSs300, FCNSs600, and CNSs samples.

Fig. S4

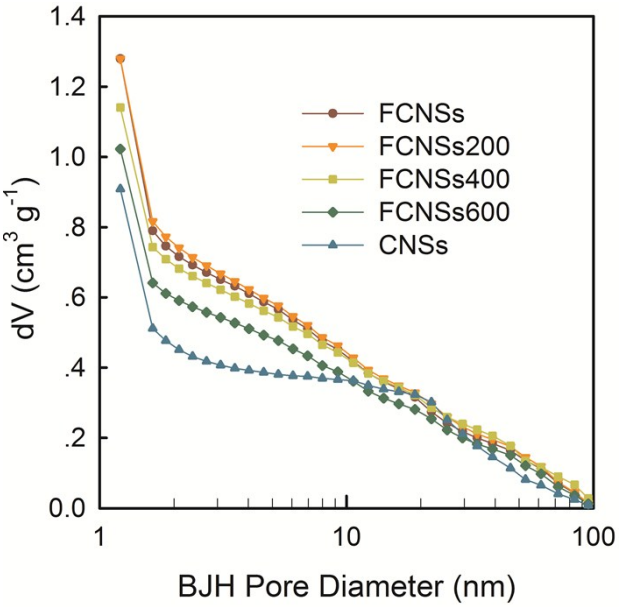

Fig. S4. The BJH PSD results of FCNSs, FCNSs200, FCNSs300, FCNSs600, and CNSs.

Fig. S5

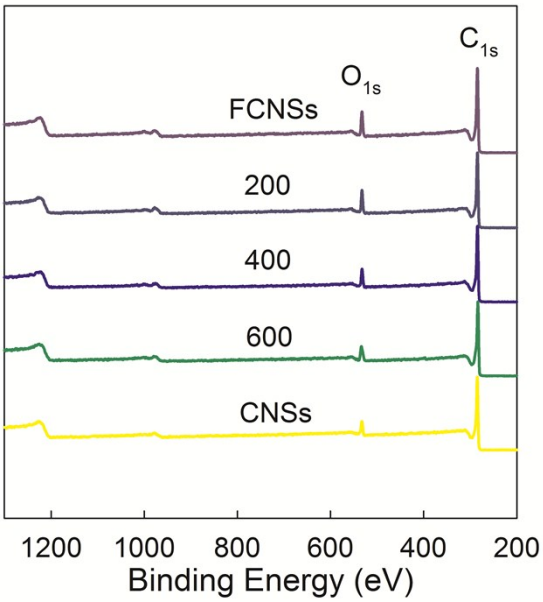

Fig. S5. Experimental XPS results of the FCNSs, FCNSs200, FCNSs300, FCNSs600, and CNSs samples.

Fig. S6

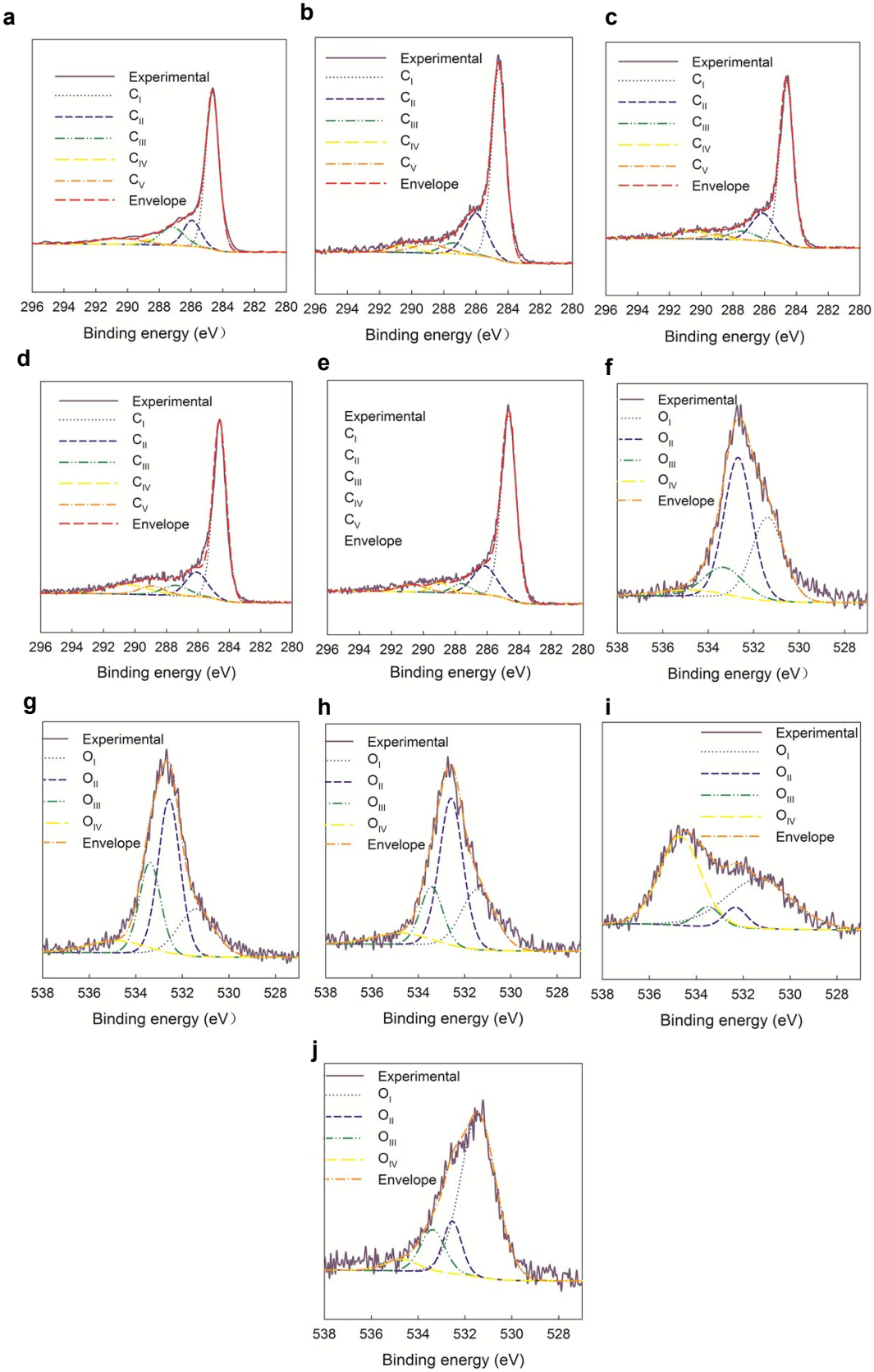

Figure S6. The corresponding C1s, deconvolution of (a) FCNSs, (b) FCNSs200, (c) FCNSs400, (d) FCNSs600, (e) CNSs. The corresponding O1s, deconvolution of (f) FCNSs, (g) FCNSs200, (h) FCNSs400, (i) FCNSs600, (j) CNSs.

Fig. S7

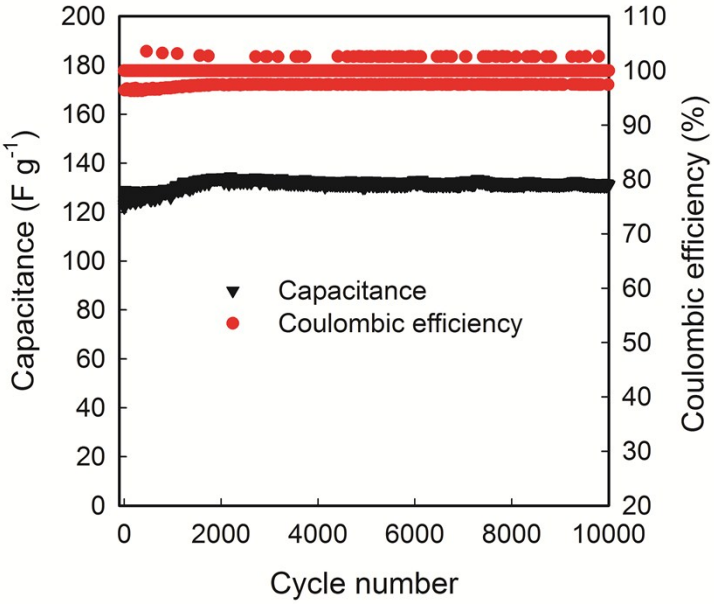

Fig. S7. Cycling stability of the FCNSs based Zn-ion hybrid SC with IL at 5 A g^{-1} for 10000 cycles of charge-discharge in a voltage window of 0.1-1.8 V.

Fig. S8

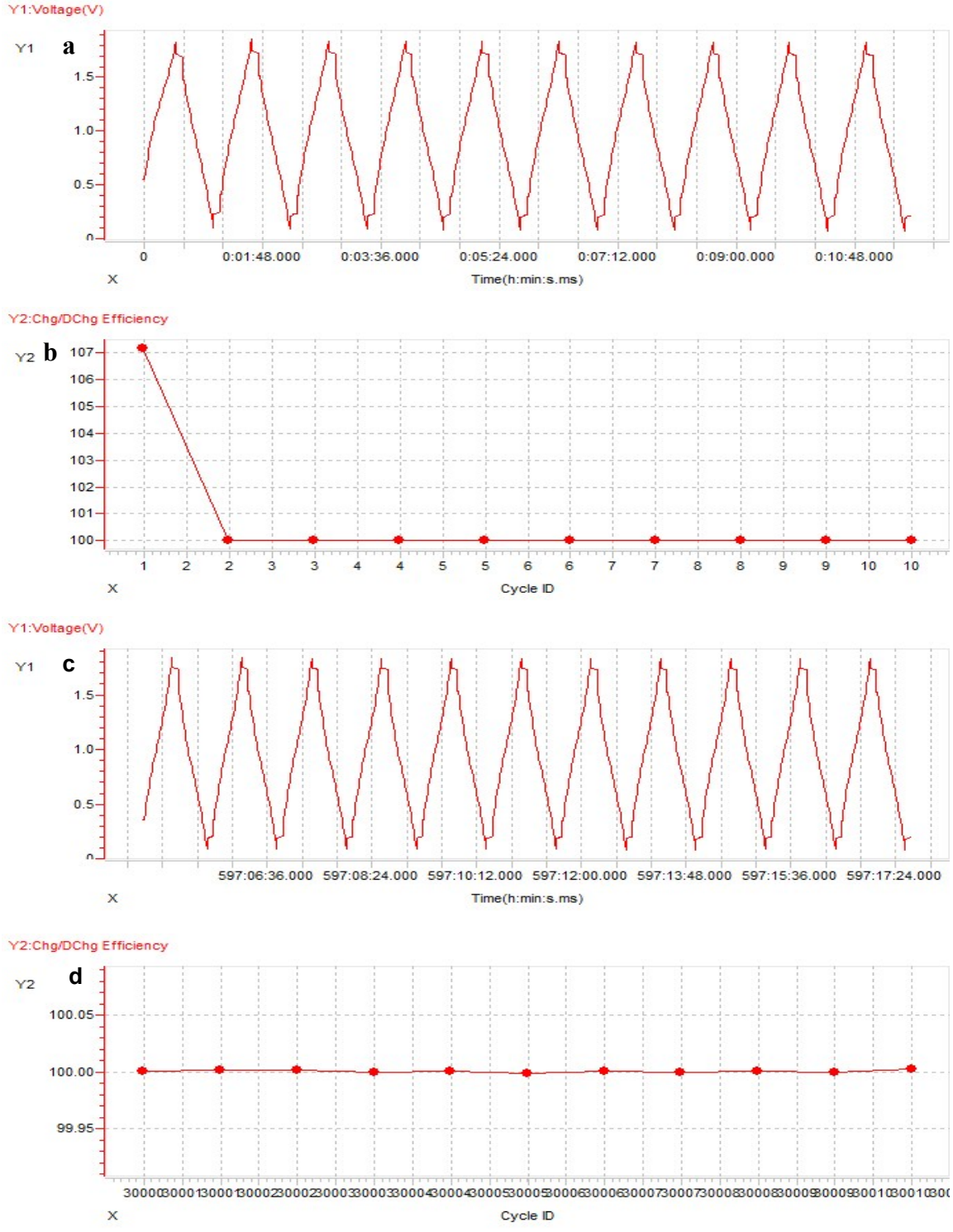
Y1:Voltage(V)
Y1
a
1.5
1.0
0.5
0
0:01:48.000
0:03:36.000
0:05:24.000
0:07:12.000
0:09:00.000
0:10:48.000
X
Time(h:min:s.ms)
Y2:Chg/DChg Efficiency
Y2
b
107
106
105
104
103
102
101
100
1 2 2 3 3 4 4 5 5 6 6 7 7 8 8 9 9 10 10
X
Cycle ID
Y1:Voltage(V)
Y1
c
1.5
1.0
0.5
0
597:06:36.000
597:08:24.000
597:10:12.000
597:12:00.000
597:13:48.000
597:15:36.000
597:17:24.000
X
Time(h:min:s.ms)
Y2:Chg/DChg Efficiency
Y2
d
100.05
100.00
99.95
X
Cycle ID

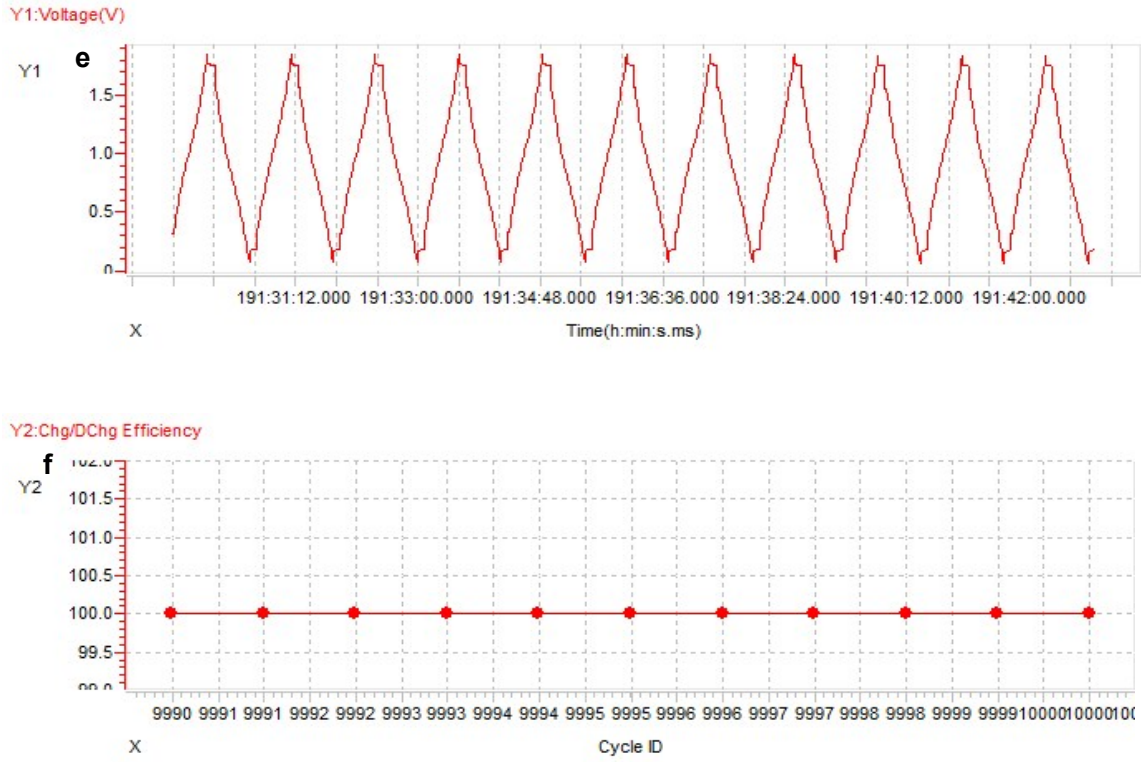

Fig. S8. Recorded cycling results of the FCNSs based Zn-ion hybrid SC with AN at 10 A g^{-1} based on the mass of FCNSs. A rest step time of 6 seconds is set between the charge and discharge. GCD curves (a) and coulombic efficiencies (b) of the SCs from 1st to 10th cycles. GCD curves (c) and coulombic efficiencies (d) of the SCs from 30000th to 30010th cycles. GCD curves (e) and coulombic efficiencies (f) of the SCs from 59990th to 60000th cycles. It should be noted here that the NEWARE software only can record 50000 cycles. So the 50001st to 60000th cycles were recorded in the other file.

Fig. S9

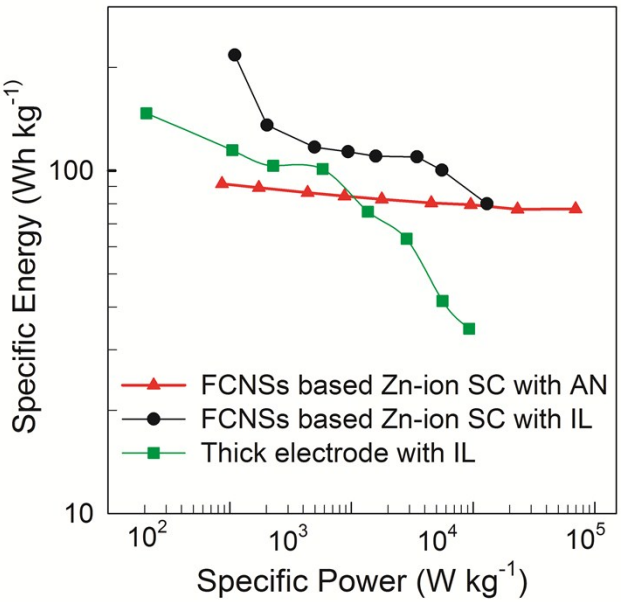

Fig. S9. Gravimetric Ragone plots of the Zn-ion hybrid SCs with both IL and AN, and the Zn-ion hybrid SCs with thick electrode (100 μm) in IL based on the mass of FCNSs positive electrode materials.

Fig. S10

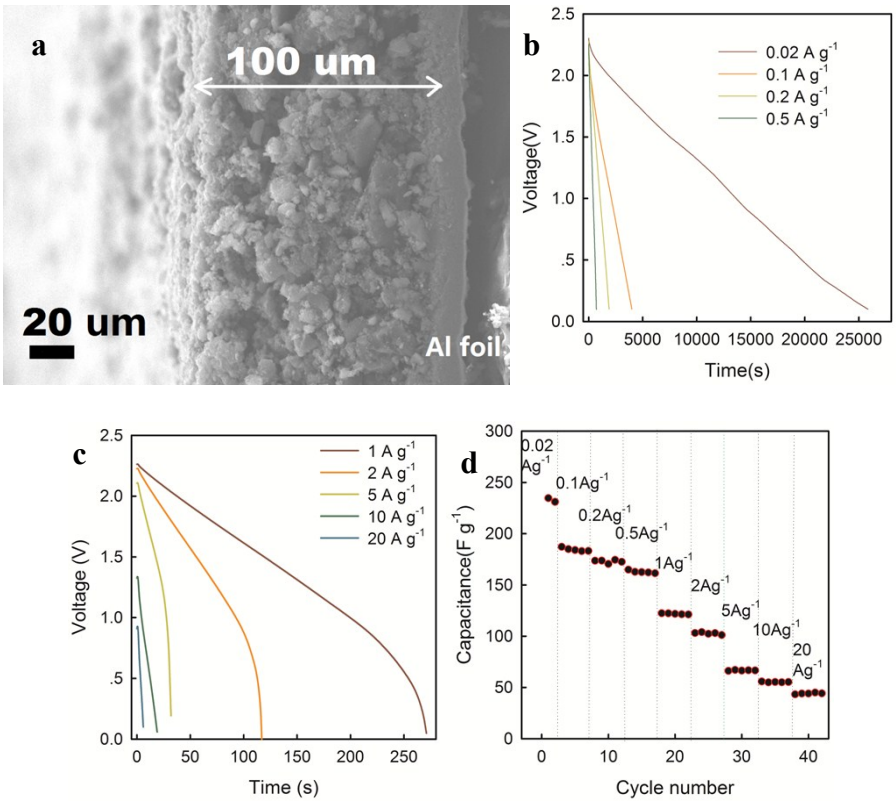

Fig. S10. The electrochemical performance of the Zn-ion hybrid SC with thick carbon electrode (100μm, high loading of 4.5 mg cm^{-2}). (a) SEM image of the cross section of the thick electrode. (b) and (c) Discharge curves at 0.02, 0.1, 0.2, 0.5, 1, 2, 5, 10, and 20 A g^{-1}. (d) The rate capability.

Table S1. Parameters of porous structure calculated from nitrogen adsorption isotherms and corresponding SC capacitances of the samples at low and high current densities.

Samples	BET SSA（m^2 /g）	BJH mesopores SSA（m^2/g）and ratio(%)	Micropores SSA ratio（% ）	Average pore size (nm)	NLDFT pore volume (cm^3 g^{-1})
FCNSs	2358	1070 (45%)	55%	3.125	1.768
FCNSs200	2403	1039 (43%)	57%	3.122	1.781
FCNSs400	2067	888 (43%)	57%	3.207	1.628
FCNSs600	2057	825 (40%)	60%	3.038	1.464
CNSs	2735	809 (30%)	70%	2.515	1.615

Table S2. Elemental analysis of the five samples.

Sample	The weight loss ratio after heat treatment(%)	Content of element, ω (%)			
		C	H	N	O[a)]
FCNSs	-	88.30	1.04	0.72	9.90
FCNSs200	~7.8	88.70	1.04	0.71	9.60
FCNSs400	~8.1	89.20	1.15	0.75	8.90
FCNSs600	~8.5	90.10	0.93	0.72	8.30
CNSs	-	93.70	0.48	0.36	5.46

[a)] Calculated value. ω (O)=100%-ω (H)- ω (C)- ω (N)

Table S3. Summarization of different oxygen containing groups on the surface of FCNSs,

Atom type	Peak label	Peak position/ eV	Group	Percentage (%)				
				FCNSs	200	400	600	CNSs
C_{1s}	C_I	284.6	Graphitized carbon	58.2	62	63.7	62.9	67.5
	C_{II}	286.1	C–OH	28.8	21	17.9	13.7	16.5
	C_{III}	287.4	C=O	1.4	5.9	6.7	7.2	4.5
	C_{IV}	288.9	O=C-O	3.6	4.2	3.5	10.7	6.4
	C_V	290.6	Carbonate groups	8.0	6.9	8.1	5.8	5.1
O1s	O_I	531.4	C=O	24.0	21.8	27.1	41.6	70.5
	O_{II}	532.5	C=O and C–OH	49.8	44.2	47.0	5.9	12
	O_{III}	533.4	C-O-C and C–OH	19.4	25.1	17.5	6.2	13
	O_{IV}	534.8	C=O in carboxyl	6.8	8.9	8.2	46.3	4.6

FCNSs200, FCNSs400, FCNSs600, and CNSs based on the XPS deconvolution results.

Table S4. Comparison of the electrochemical performances of the dual-ion and Zn-ion energy storage devices.

Type	cathode	anode	Electrolyte	capacity	Voltage	Cyclic	Rate	Energy	Power	Refs.
Na^+	3D nanoporous carbon	TiO_2/C	$NaClO_4$ in 1:1 v/v EC and PC with 5 wt% FEC	218.4 F g^{-1} at 0.1 A g^{-1}	4V	10000 cycles (90%, at 1 A g^{-1})	38.4 F g^{-1} at 10 A g^{-1}	142.7 Wh kg^{-1} at 250 W kg^{-1}	25 kW kg^{-1} with 61.8 Wh kg^{-1}	6
K^+	AC (Kuraray)	Soft carbon	3 M KFSI in DME	214 mAh g^{-1} at 500 mA g^{-1}	4V	1000 cycles (71.4% ,at 350 mA g^{-1}).	13.3 Wh kg^{-1} at 700 mAg^{-1}	120 Wh kg^{-1} at 96 W kg^{-1}	599 W kg^{-1} with 13.3 Wh kg^{-1}	7
Mg^{2+}	Mg-OMS-2/Graphene	Mg	0.5 M $Mg(NO_3)_2$ aqueous solution	232 mAh g^{-1} at 20 mA g^{-1}	2V	500 cycles (95.8%, at 100 mA g^{-1})	232.4 mAh g^{-1} at 20 mA g^{-1} 50 mAh g^{-1} at 1 A g^{-1}	46.9 Wh kg^{-1} at 20 m Ag^{-1}	1800 W kg^{-1} with 25 Wh kg^{-1}	8
Al^{3+}	Graphitic-foam	Al	1.3 M $AlCl_3$ in [EMIm]Cl	70 mAh g^{-1} at 1 A g^{-1}	2.45V	7,500 cycles (without capacity decay at 4 A g^{-1})	65 mAh g^{-1} at 5 Ag^{-1}	40 Wh kg^{-1} at 3000 W kg^{-1}	3000 W kg^{-1}	9
Zn^{2+}	AC	Zn	2 M $ZnSO_4$ aqueous solution	121 mAh g^{-1} at 0.1 A g^{-1}	1.8V	10000 cycles（91% at 1A g^{-1}）	121mAh g^{-1} at 100 mA g^{-1}, 41 mAh g^{-1} at 20A g^{-1}	84 Wh kg^{-1} at a 69 W kg^{-1}	14.9 kW kg^{-1} with 30 Wh kg^{-1}	10
	AC (KOH activated Coconut shells)	Zn	1 M $Zn(CF_3SO_3)_2$ in An	170 F g^{-1} at 0.1 A g^{-1}	1.8V	20000 cycles（91% at 2 A g^{-1}）	85% capacitance retention at 2 A g^{-1}	69 Wh kg^{-1} at 0.1 A g^{-1}	1725 W kg^{-1} at 52.7 Wh kg^{-1}	11

Zn^{2+}	α-MnO_2/CNT	Flexible Zn anode	AF-gel electrolyte containing 2 mol L^{-1} $ZnSO_4$ and 0.1 mol L^{-1} $MnSO_4$	275 mA h g^{-1} at 0.2 A g^{-1}	1.8V	600 cycles (85% at 2.4 A g^{-1})	88.36 % (243 mAh g^{-1}) at 0 ˚C and 82.18 % at -20 ˚C	32.8 Wh L^{-1} at 23.7 W L^{-1}		[12]
Zn^{2+}	MoS_2 nanosheets	Zn deposited on carbon cloth	2 M aqueous $ZnSO_4$ solution	202.6 mA h g^{-1} at 0.1 A g^{-1}	1.5V	600 cycles, (98.6% at 1 A g^{-1})	52% capacitance retention at 4 A g^{-1}	148.2 Wh kg^{-1} 70.5 W kg^{-1}		[13]
this work	FCNSs	Zn	0.2 M $Zn(CF_3SO_3)_2$ in $EMIMCF_3SO_3$	300 F g^{-1} at 0.1 A g^{-1}, 198 F g^{-1} at 0.2 A g^{-1}	2.4V	35000 cycles（82% at 5 A g^{-1}）	64% capacitance retention at 20 A g^{-1}	217 Wh kg^{-1} at 109 W kg^{-1}	13 kW kg^{-1} with 79 Wh kg^{-1}	
this work	FCNSs	Zn	1 M $Zn(CF_3SO_3)_2$ in AN	226 F g^{-1} at 0.1 A g^{-1}	1.8V	60000 cycles (without capancitance decay at 10 A g^{-1})	84% capacitance retention at 50 A g^{-1}	92 Wh kg^{-1} at 86 W kg^{-1}	56 kW kg^{-1} with 77 Wh kg^{-1}	

References

1. H.-C. Wu, H.-C. Wu, E. Lee and N.-L. Wu, *Electrochem. Commun.*, 2010, **12**, 488-491.
2. J. P. Perdew, M. Ernzerhof and K. Burke, *The Journal of Chemical Physics*, 1996, **105**, 9982-9985.
3. G. Kresse and J. Furthmüller, *Phys Rev B*, 1996, **54**, 11169-11186.
4. G. Kresse and J. Furthmüller, *Comp Mater Sci*, 1996, **6**, 15-50.
5. F. Vincenzo and M. Methfessel, *J. Phys.: Condens. Matter*, 1996, **8**, 6525.
6. E. Lim, C. Jo, M. S. Kim, M.-H. Kim, J. Chun, H. Kim, J. Park, K. C. Roh, K. Kang, S. Yoon and J. Lee, *Adv. Funct. Mater.*, 2016, **26**, 3711-3719.
7. L. Fan, K. Lin, J. Wang, R. Ma and B. Lu, *Adv. Mater.*, 2018, **30**, 1800804.
8. H. Zhang, K. Ye, K. Zhu, R. Cang, X. Wang, G. Wang and D. Cao, *ACS Sustainable Chemistry & Engineering*, 2017, **5**, 6727-6735.
9. M.-C. Lin, M. Gong, B. Lu, Y. Wu, D.-Y. Wang, M. Guan, M. Angell, C. Chen, J. Yang, B.-J. Hwang and H. Dai, *Nature*, 2015, **520**, 324.
10. L. Dong, X. Ma, Y. Li, L. Zhao, W. Liu, J. Cheng, C. Xu, B. Li, Q.-H. Yang and F. Kang, *Energy Storage Materials*, 2018, **13**, 96-102.
11. H. Wang, M. Wang and Y. Tang, *Energy Storage Materials*, 2018, **13**, 1-7.
12. F. Mo, G. Liang, Q. Meng, Z. Liu, H. Li, J. Fan and C. Zhi, *Energy & Environ. Sci.*, 2019, **12**, 706-715.
13. H. Li, Q. Yang, F. Mo, G. Liang, Z. Liu, Z. Tang, L. Ma, J. Liu, Z. Shi and C. Zhi, *Energy Storage Materials*, 2018, DOI: https://doi.org/10.1016/j.ensm.2018.10.005.